

# Multi-interactive Siamese Decoder for RGBT Salient Object Detection

Zhengzheng Tu, Zhun Li, Chenglong Li, Yang Lang, and Jin Tang

**Abstract**—RGBT salient object detection (SOD) aims to segment the common prominent regions of visible and thermal infrared images. Existing RGBT SOD methods don't fully explore and exploit the potentials of complementarity of different modalities and the global context of image contents, which play a vital role in achieving accurate results. In this paper, we propose a multi-interactive Siamese decoder to mine and model the multi-type interactions for accurate RGBT SOD. In specific, we first encode RGB and thermal image pair into multi-level multi-modal representation. Then, we design a novel Siamese decoder to integrate the multi-level interactions of dual modalities and global contexts. With these interactions, our method works well in diversely challenging scenarios even in the presence of invalid modality. Moreover, the Siamese decoder employs label supervision to drive feature learning in each modality and the modality prejudice is thus suppressed. Finally, we carry out extensive experiments on several benchmark datasets, and the results show that the proposed method achieves the outstanding performance against state-of-the-art algorithms. The source code has released at: <https://github.com/lz118/Multi-interactive-Siamese-Decoder>.

**Index Terms**—Salient object detection, Information fusion, Siamese decoder, Multiple interactions

## I. INTRODUCTION

**R**GBT salient object detection (SOD) aims at estimating the common conspicuous objects or regions in an aligned visible and thermal infrared image pair. It differs the task of RGBD SOD as follows. RGBD SOD aims to introduce depth information as an auxiliary modality to encounter some difficulties such as similar foreground and cluttered background. As the depth information can catch the distance between objects and camera, it can easily distinguish salient object from similar objects and cluttered background. Therefore, existing RGBD SOD methods mainly focus on how to explore depth information to complement RGB one. While RGBT SOD treats RGB and thermal modalities equally and its target is to leverage complementary advantages to discover common conspicuous objects in both modalities, similar to other computer vision tasks, such as RGBT tracking [1], [2] and multi-spectral person re-identification [3], [4]. RGBT SOD is more meaningful than single-modality SOD and RGBD SOD in some practical applications such as automatic driving in foggy weather and nighttime, and abnormal detection in important places like power stations.

This work is partly supported by Major Project for New Generation of AI (No. 2018AAA0100400), National Natural Science Foundation of China (No. 61976003), Key Project of Research and Development of Anhui Province (No. 201904b11020037).

The authors are with Key Lab of Intelligent Computing and Signal Processing of Ministry of Education, Anhui Provincial Key Laboratory of Multimodal Cognitive Computation, School of Computer Science and Technology, Anhui University, Hefei 230601, China

Existing works have explored the task of RGBT SOD to some extent. Wang et al. [5] propose a multi-task manifold ranking algorithm, which introduces a weight for each modality to describe the reliability and then adaptively fuses two modalities with these weights. Based on [5], Tang et al. [6] further take both of collaboration and heterogeneity into account to make more effective fusion of different modalities. Tu et al. [7] propose a collaborative graph learning algorithm to integrate multi-level deep features. However, handcraft features can not represent the semantic relevance between pixels well, and the superpixel-based methods require robust superpixel segmentation results. Thus the above-mentioned graph-based RGBT SOD methods can hardly maintain good performances on various challenges.

In recent years, deep learning has shown the superior ability of feature representation. Tu et al. [8] provide an effective baseline method for RGBT SOD, which aggregates multi-level multi-modal features with attention mechanism, and shows great improvement against the previous methods. Zhang et al. [9] propose an end-to-end deep neural network by fusing multi-modal information at various stages. They design several modules embedded into network to effectively fuse multi-modal deep features for robust saliency computing. However, there are two key problems not addressed well. One is to suppress modality prejudice which means we should focus on common conspicuous regions and avoid dominated results by one modality. The other is how to achieve effective complementation between modalities and prevent noise interference.

In this work, we propose a novel deep CNN model called multi-interactive Siamese decoder for RGBT SOD. To handle the first problem, we design a Siamese decoder architecture whose two branches decode for two modalities respectively. We set two prediction heads on the top of Siamese decoder to compute saliency maps of two modalities, and employ label supervision to drive feature learning in each modality. The modality prejudice can thus be suppressed since the label is identical on two modalities. With the supervision driven, two decoder branches trend to discover common salient regions from two modalities. The output features from Siamese decoder are fused to predict the final saliency map and the common conspicuous regions can thus be highlighted.

To handle the second problem, we design a multi-interaction block (MIB) to model the interactions of dual modalities, multi-level features and global contexts. On the one hand, we adopt modality interaction between two branches and therefore they can learn from each other to complement themselves. On the other hand, we also interact global contexts and multi-level features in Siamese decoder. The former is helpful for

locating the salient regions and holding back the background noises, while the latter aims at supplying the spatial details for recovering the high-resolution results. Particularly, we embed three MIBs on each stream of Siamese decoder to decode features in a progressive way. Each MIB receives three inputs including the output of previous MIB, the encoded multi-level features of modalities and the information of global contexts.

Such design has the following major properties. 1) It propagates the useful complementary features of dual modalities to each other, and the good performance can be achieved even though one modality is invalid or with many noises. 2) It captures the hierarchical encoded features to restore more spatial details. The up-sampled decoded features can be complemented by the details and thus achieve clearer structure of salient objects. 3) It accepts global context to help highlighting complete salient regions. The global context contains strong semantic relevance of pixels within and between modalities, and is thus helpful for locating salient objects and hold back background noises.

To make the Siamese decoder more robust to the problem that one modality is invalid or with many noises, we develop a data augmentation strategy. In specific, we randomly replace the input of a modality with zero or a noise map sampled in standard normal distribution. By this way, the proposed network can be trained to adapt this situation.

The contributions of this paper are summarized as follows.

- We propose a novel end-to-end trained multi-interaction Siamese decoder network to fully suppress modality bias and exploit modality complementarity in RGBT SOD.
- We design an effective multi-interaction model to utilize multi-type cues including dual modalities, hierarchical features and global contexts to perform more accurate RGBT SOD.
- A simple yet effective data augmentation strategy is designed to train the proposed network, and the performance is thus further boosted in the presence of invalid or unreliable modalities.
- Extensive experiments on several public datasets show that the proposed method achieves the state-of-the-art performance against the existing methods.

## II. RELATED WORK

### A. Salient Object Detection

In recent years, deep learning-based methods have achieved great progress in salient object detection. Wang et al. [10] utilize the neural network to perform the fusion of local spatial features and global semantic features, then combine local estimation with global search to predict saliency map. Liu et al. [11] design a deep hierarchical network to predict a coarse saliency map and then refine it hierarchically and progressively. Next, many researches come out based on fully convolutional network with its successful applications in semantic segmentation. Wang et al. [12] propose a recurrent FCN to constantly refine the saliency. Hou et al. [13] add several short connections from the deeper side output to the shallower side output for enhancing more accuracy. Luo et al. [14] aggregate hierarchical features and contrast features to

generate local saliency map, and then use the global semantic features to polish it. Liu et al. [15] propose a novel pixel-level context-aware network that learns to pay selective attention to the context information of each pixel. Deng et al. [16] propose a module to learn the residual between the intermediate saliency prediction and the ground truth by alternatively using the low-level features and the high-level features. Wu et al. [17] design a cascaded partial decoder for fast and accurate salient object detection. Zhao et al. [18] introduce edge detection to SOD for more accurate boundaries. Wei et al. [19] design a reasonable module to aggregate hierarchical features effectively and propose a weighted binary cross entropy loss function to emphasize the region that is difficult to predict. Numerous studies have made SOD algorithms more robust. However, with existing algorithms, it is difficult to deal with some challenges such as bad imaging conditions, which might cause defects or semantic ambiguity in visible images.

### B. RGBT Salient Object Detection

With the availability of thermal sensors, many works [20], [21] introduce the thermal infrared images in SOD by utilizing their complementary information. As the original work, Wang et al. [5] construct the first RGBT SOD dataset and propose a multi-task manifold ranking algorithm. Tu et al. [22] use a multi-modal multi-scale manifold ranking to achieve the fusion of different features and introduce an intermediate variable to infer the optimal ranking seeds. Furthermore, Tu et al. [7] propose a collaborative graph learning method for RGBT SOD, which takes the superpixel as the graph node and uses hierarchical deep features to learn the graph affinity and node saliency. These RGBT SOD methods use traditional machine learning technologies, which has limited capability for feature representation. As the deep learning based methods show excellent performance on SOD task, Tu et al. [8] propose an effective baseline method for RGBT SOD, which aggregates multi-level multi-modal features with attention mechanism, and shows great improvement against the previous methods. Zhang et al. [9] propose an end-to-end deep neural network by fusing multi-modal information at various stages. In this paper, we propose a more suitable network with multi-interaction Siamese decoder to utilize the multi-type cues in a reasonable way and take the modalities bias into account simultaneously.

### C. RGBD Salient Object Detection

Existing RGBD SOD methods can be divided into two categories. The mainstream one [23], [24], [25], [26], [27] uses depth maps as auxiliary information while the other one [28], [29], [30], [31], [32] regards depth maps in an equivalent way to visible image. The latter researches are similar to RGBT SOD and thus we only introduce the RGBD methods which use two modalities in an equivalent way.

Qu et al. [33] design the handcraft features of multi-modality inputs and then use them as the input of network to predict saliency maps. Song et al. [34] also use the multi-modality inputs to design kinds of features and exploit low-level feature contrasts, mid-level feature weighted factors and high-level location priors to calculate saliency measures. Liu et

al. [35] directly concatenate the modalities as a four-channel input, and then feed it to an encoder to obtain hierarchical feature representations. Finally, they use a depth recurrent network to render salient object outline from deep to shallow hierarchically and progressively.

In contrast to early fusion, the middle fusion strategy has more extensive researches. Many existing RGBD SOD methods adopt this kind of strategy to make full fusion of modalities. Liu et al. [29] perform the fusion during the decoding phase by directly adding the features of two modalities with the feature from the previous decoding step. Instead of directly adding together, Chen et al. [31] design a complementarity-aware fusion module to fuse the features of two modalities. Chen et al. [30] further propose a three-stream attention-aware network, in which a fusion stream is introduced that accompanies RGB-specific stream and depth-specific stream to obtain the new fused features for each layer, then the fused features are used for decoding. Piao et al. [25] extract multi-level complementary RGB and depth features and then fuse them by using residual connections. Then they model the relationship between depth information and object scales, and use a new recursive attention module to generate more accurate saliency maps. More recently, Fu et al. [32] use a siamese network to extract features of two modalities and propose a densely-cooperative fusion strategy. The middle fusion based method can effectively fuse encoded features, which has a great potential to be exploited. Therefore in this paper, we make a novel exploration for middle fusion strategy with a multi-interactive Siamese decoder to achieve robust RGBT SOD.

### III. MULTI-INTERACTIVE SIAMESE DECODER NETWORK

In this section, we present our multi-interactive Siamese decoder network for RGBT SOD.

#### A. Overall Architecture

As shown in Fig. 1, we use two independent backbones to extract features from RGB images and thermal infrared images respectively. Then the global information module can combine the highest-level features of two modalities to obtain the global features with various receptive fields, which are then used as global contexts for accurate location of salient regions. In the decoding phase, we adopt a Siamese decoder based on two modalities to achieve saliency computing progressively. To be specific, we design the multi-interaction block (MIB) and then embed it into the Siamese decoder in a cascade way to achieve sufficient fusion by multi-type cues. Intuitively, we make two outputs of the Siamese decoder be consistent by using the same saliency supervision. Therefore the joint computation is achieved in the progressive interactive decoding phase, while the prejudice and noise of two modalities are suppressed. Finally, we fuse the final features of Siamese decoder to predict the final saliency map. Details of each part are presented in the following subsections.

#### B. Encoder Network

For universality and simplicity, we use VGG16 [36] as our encoder to extract hierarchical features with different resolutions from the images of two modalities. Herein, we remove the last pooling layer and two fully connected layers in VGG16. As we know, features from the deeper layer encode high-level semantic information while features from the shallower layer contain more spatial details. The features from the shallowest layer contain lots of details of foreground and background which may be regarded as noise and be harmful for salient object detection. Besides, the resolution of these features is the same as the input image, and adopting these features has a high computational complexity. To improve the efficiency and performance, we abandon these features of two modalities. For convenience, the remaining features extracted from RGB image are denoted as  $R_2 \sim R_5$  and those from thermal infrared image are denoted as  $T_2 \sim T_5$ .

#### C. Global Information Module

Global context is vital for locating the regions in RGBT SOD task. Region based context is helpful for maintaining the completeness of salient region and suppressing background noise. Therefore we should extract the global features with multiple receptive fields for performance boosting. Inspired by the pyramid pooling module (PPM) [37] which is widely used in capturing multiple region contexts, we simply change PPM and then embed it into our network. The details can be seen in the bottom right of Fig. 1. We collect the top encoded features of two modalities ( $R_5$  and  $T_5$ ) and then concatenate them in a channel-wise way. A channel attention mechanism is used for selective recombination of the two features. For simplification, we implement the channel attention by CBAM [38] and replace the multiple perceptrons in CBAM by  $1 * 1$  convolution layer together with batch normalization [39] and Relu [40] activation function followed. The channel attention is marked as  $CA(*)$ . The combination of convolution layer, batch normalization and Relu is marked as  $Conv(*)$  for convenience. We adopt a convolutional block to decrease the channel number to 256, and the output is marked as  $F$ :

$$F = Conv(CA([R_5, T_5])) \quad (1)$$

where  $[*]$  is the channel-wise concatenation. Then four operations of adaptive global max pooling with different sizes are used to obtain four feature maps with different receptive fields. We use four convolutional blocks to reconstruct four feature maps respectively. After that, we up-sample all the four feature maps to the size of  $F$  and then concatenate them with  $F$ . Finally, we apply a convolutional layer to the concatenated features and generate the reconstructed features  $G$  which contain the information from the global receptive field.

$$\tilde{F}_i = UP(Conv(MaxPooling_n(F))) \quad (2)$$

$$G = Conv([\tilde{F}_i]), i = 1, \dots, 4 \quad (3)$$

where  $UP(*)$  is the up-sampling operation and  $MaxPooling_n(*)$  is an adaptive max pooling with  $n * n$



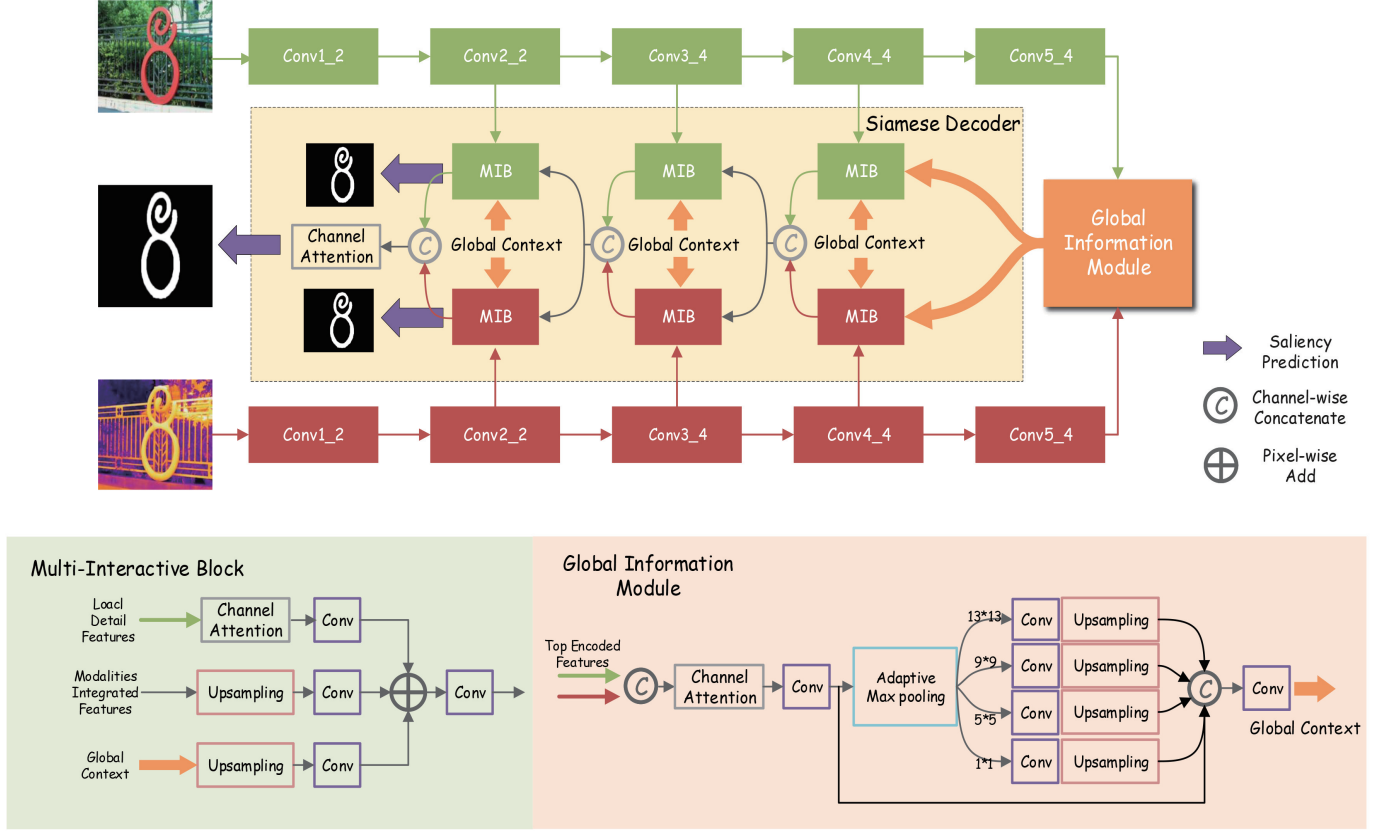


Fig. 1. Framework of our proposed method. The RGB image related parts are painted in blue and the thermal image related parts are painted in red. The global information is painted in green. The 'Score' block is a convolutional layer with  $1 \times 1$  kernel size and outputs predicted saliency map with single channel.

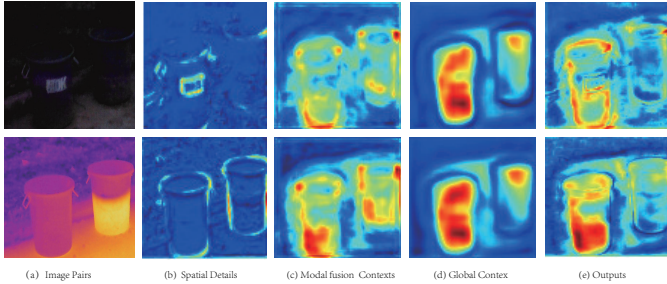


Fig. 2. Feature visualization in the second group MIBs in Siamese decoder. We average the feature maps in a channel-wise manner. (a) Input image pairs. (b) Spatial details ( $\tilde{A}_i$ ) computed by encoded features ( $A_i$ ). (c) Fused features of modalities ( $\tilde{M}_i$ ). (d) Global contexts ( $\tilde{G}_i$ ) adjusted to MIB. (e) Outputs of MIBs in two branches.

output size.  $\tilde{F}_i$  represents the  $i$ -th branch's output where  $i = 1, 2, 3, 4$  with  $n = 1, 5, 9, 13$  respectively. And the output  $G$  is the global contexts shown in Fig. 1.

#### D. Siamese Decoder Network

As RGBT SOD has its particularity that focusing on common conspicuous objects in two modalities, the joint computation should be considered. Besides achieving the complementarity of two modalities, the abilities of eliminating the prejudice and exploring the commonalities should also be possessed. Thus we design a Siamese decoder with multi-type

cues to solve these problems. The architecture of our Siamese decoder can be seen in Fig. 1. In general, the hierarchical encoded features are always useful for the up-sampling of decoded features. And the global context is vital for region location. Therefore, we adopt a multi-interactive manner to make full use of multi-type cues. Specially, we design a multi-interaction block (MIB) and embed it into the decoder in a cascade way, which can achieve the interactions of dual modalities, hierarchical features and global contexts. The details of MIB are shown as the bottom left of Fig. 1. In this subsection, we will focus on the three kinds of interactions to present MIB and Siamese decoder.

1) *Interaction with hierarchical features:* In each decoder stream, we use the encoded features to restore the spatial details step by step. We use the channel attention to emphasize the more useful features, and then decrease the number of channels to 128.

$$\tilde{A}_i = \text{Conv}(\text{CA}(A_i)), i = 2, 3, 4 \quad (4)$$

where  $A_i$  represents the corresponding RGB encoded features  $R_i$  or the thermal encoded features  $T_i$ . The corresponding encoded features in current decode stream are used for refining the spatial details of the previous output which has been up-sampled. Because of adopting the encoded features in specific modality, the outputs of the two decode streams can maintain strong characteristics of corresponding modalities. Thus we

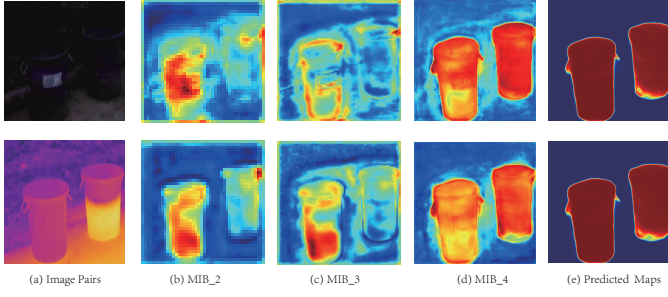


Fig. 3. Visualization of all MIBs' outputs and the final predicted saliency maps of Siamese decoder. The presented feature maps are averaged in a channel-wise way. Herein,  $MIB\_i$  is the group of MIBs corresponding to the  $i$ -th level encoded features.

can effectively prevent the useful details from fading away after the fusion step. For example, in Figure 2, we visualize the spatial details used in the second group MIBs in Siamese decoder. From the maps in the column (b), we can see there are abundant details in encoded features of shallower layers. And in column (e), the modality characteristic that having abundant details is maintained.

2) *Interaction with dual modalities:* For the interactions of dual modalities, we concatenate the previous MIB outputs from two decoders marked as  $M_i$ . These output features contain previous fused information and the specific information of two modalities. In the top-down path, they are regarded as high-level semantic features with strong relevance of pixels. Then we use the channel attention to adaptively select useful information and achieve the feature reconstruction from the concatenated features. We up-sample the reconstructed features to the size as same as  $A_i$  and adopt a convolutional block to reduce the number of channels of reconstructed features to 128. Thus, we get  $\tilde{M}_i$ .

$$\tilde{M}_i = Conv(UP(CA(M_i))), i = 2, 3, 4 \quad (5)$$

Here, we make the fusion of modalities by a channel attention because we want to prevent the multi-modal information from excessive disturbance by each other. And we think the decoder can implicitly achieve the complementarity between modalities as the Siamese decoder is driven by the same saliency supervision. In Fig. 2, the third column shows the fused features of the modalities in the second group MIBs. We can see that the deficient features in RGB modality have been complemented by the thermal modality. And the features will be polished to be better in subsequent steps in the decoder.

3) *Interaction with global contexts:* In the top-down path, with the fusion of the spatial details, the location of the object will be gradually diluted [41]. Besides, although the high-level encoded features model the semantic relevance in pixels, the receptive field of VGG16 is too small so that the network cannot obtain sufficient semantic information, which might lead to missing some parts of big object or multiple objects. To handle these problems, we design the global information module as Section. III-C introduced.  $G$  is the global context computed by global information module. We integrate it into each MIB to maintain the location of salient region. In detail, we up-sample  $G$  to the size of  $A_i$  and use a convolutional

block to decrease the number of channels to 128. Therefore the global context can be adjusted to interact with other information.

$$\tilde{G}_i = Conv(UP(G)), i = 2, 3, 4 \quad (6)$$

Obviously, in Fig. 2 we can find that the global context effectively highlights the salient region. With the global context interacted, the main part of salient region is emphasized and the noise of background is suppressed.

4) *Integration of multi-type cues:* We sum the above three kinds of features directly and obtain the reconstructed fused features  $Z$  through a convolutional block as the output of a MIB:

$$Z_i = Conv(\tilde{M}_i + \tilde{G}_i + \tilde{A}_i), i = 2, 3, 4 \quad (7)$$

On the one hand, the pixel-wise addition does not need any parameter and the calculation is simple and efficient. On the other hand, the operation of pixel-wise addition means that we treat these features equally, which avoid the network learning a bias on one kind of features.

Other MIBs have the same operation except for different inputs. It should be noted that the interactions with dual modalities only perform on the outputs of previous MIBs in two paths, and we still use the original features of the dual modalities to obtain the low-level spatial details. Therefore, the final features from both of decoders can effectively maintain the characteristics of the corresponding modality to some extent and also contain valid information. Through the three steps of cascaded decoder, the interactions of dual modalities, hierarchical features and global contexts can be performed well, and the resolution of the last MIB's output will be restored to 1/4 of the input image.

Finally, we fuse the final features from MIBs in Siamese decoder by the concatenation and a simple channel-wise attention to predict the final saliency map. And then we up-sample the saliency map four times to the same size of the input image, marked as  $S_f$ . Besides, we also use these outputted features to predict two branches of saliency maps respectively with the same supervision operation. Therefore, although the two branches of Siamese decoder receive different type of cues, they trend to infer the same salient regions, benefited from the interactions in Siamese decoder. By this way, we can explore the complementarity of dual modalities and eliminate their prejudice.

We visualize the whole procedure of Siamese decoder in Fig. 3. We can see that the outputs of MIBs are gradually improved with more accurate details. And the features in two branch are trending to be consistent, which verifies the ability of our network for complementarity of modalities and eliminating the modal prejudice.

#### E. Loss Function

Given the predicted saliency map  $S = \{S_i | i = 1, \dots, T\}$  and the corresponding ground truth  $Y = \{Y_i | i = 1, \dots, T\}$ , where  $T$  is number of total pixels, the binary cross entropy (BCE) loss commonly used in SOD task is formulated as follows:

$$\mathcal{L}(S, Y) = - \sum_{i=1}^T (Y_i * \log(S_i) + (1 - Y_i) * \log(1 - S_i)) \quad (8)$$

We predict two saliency maps from the two branches of Siamese decoder denoted as  $S_1$  and  $S_2$ , and then compute the BCE loss with the ground truth  $Y$ :

$$\mathcal{L}_d = \mathcal{L}(S_1, Y) + \mathcal{L}(S_2, Y) \quad (9)$$

To make the global information module be learned better, we predict a saliency map  $S_g$  from the global context  $G$ . For the same size, we down-sample  $Y$  with the factor of 16 to obtain  $Y_g$ . Then, a BCE loss is used:

$$\mathcal{L}_g = - \sum_{i=1}^{T_g} (Y_{gi} * \log(S_{gi}) + (1 - Y_{gi}) * \log(1 - S_{gi})) \quad (10)$$

where the  $T_g$  is the number of total pixels of  $S_g$ . For the final predicted map  $S_f$ , the loss function is:

$$\mathcal{L}_f = \mathcal{L}(S_f, Y) \quad (11)$$

Furthermore, we use the smoothness loss [42] as a constraint to achieve region consistency and obtain clearer edges. We compute first-order derivatives of the saliency map in the smoothness term as [43] does.

$$\mathcal{L}_s = \sum_{i=1}^T \sum_{d \in \vec{x}, \vec{y}} \Psi \left( |\partial_d S_{fi}| e^{-\alpha |\partial_d Y_i|} \right) \quad (12)$$

$$\Psi(s) = \sqrt{s^2 + 1e^{-6}} \quad (13)$$

where  $\partial_d$  represents the partial derivatives on  $\vec{x}$  and  $\vec{y}$  directions. And we set  $\alpha = 10$  as [43] does. Therefore, our total loss is:

$$\mathcal{L} = \mathcal{L}_d + \mathcal{L}_g + \mathcal{L}_f + \beta \mathcal{L}_s \quad (14)$$

We empirically set  $\beta = 0.5$  to balance the effect of smoothness loss. Our network can be trained well with the cooperation of this four kinds of constraints.

#### F. Noisy Data Augmentation

We observe that some modalities in RGBT image pairs are not always useful. For example, the RGB modality is indiscernible when the image is captured in low illumination while the thermal modality is invalid when the foreground and background have close temperature. Even in the complex scene, both of the two modalities have large noises. Therefore, we design a simple yet effective data augmentation strategy to train the proposed network. We randomly set one modality to a zero map or noisy maps sampled from the standard normal distribution. The zero map is used to simulate the case of one invalid modality. Therefore the network can not extract any information from it. The noisy maps are used to simulate the noise modality and the network can thus obtain many useless information. Through training on this kind of data, our network can learn to conquer these difficulties and to care more about the interaction between modalities. In our implementation, we set the probability at 10% to randomly use zero map or noisy maps. Both of two modalities have the probability of 50% to be replaced and the probability of two kinds of maps are also 50%.

## IV. EXPERIMENT

In this section, we give the details of our experiments. At first, we introduce the used datasets. Then we show the experimental setup including implementation details and evaluation metrics. Finally, we conduct and analyze the comparison experiments and ablation experiments to demonstrate the effectiveness of our method.

### A. Dataset

There are three RGBT SOD dataset publicly available, including VT821 [5], VT1000 [7] and VT5000 [8]. VT821 contains 821 registered RGBT image pairs. To strengthen the challenge of the dataset, some noises are added to some images. As RGBT image pairs in VT821 are registered manually, there are vacant regions in the thermal infrared images. VT1000 contains 1000 RGBT image pairs, with relatively simple scenes and well aligned images. VT5000 collects 5000 aligned RGBT image pairs, and has more complex scenes and various objects. There are many challenges in above datasets including big salient object (BSO), small salient object (SSO), multiple salient object (MSO), low illumination (LI), center bias (CB), cross image boundary (CIB), similar appearance (SA), thermal crossover (TC), image clutter (IC), out of focus (OF) and bad weather (BW), which basically covers all the problems in RGBT SOD. In this work, 2500 various image pairs in VT5000 are chosen as our training set, and the rest image pairs together with VT821 and VT1000 are taken as testing sets.

### B. Experimental Setup

1) *Implementation details.*: Our network is implemented based on Pytorch and trained with a single Titan Xp GPU. We use the stochastic gradient descent (SGD) to optimize parameters with the weight decay of 5e-4 and the momentum of 0.9. We train 100 epochs with batch size of 4. The initial learning rate is 1e-3, and it becomes 1e-4 after 20 epochs and 1e-5 after 50 epochs. For the input, we resize all the images to the size of 352 \* 352.

2) *Evaluation metrics.*: For evaluating different methods, we use precision-recall (PR) curve, F-measure, S-measure, E-measure [44] and mean absolute error [45], which are widely used in SOD.

The formula of F-measure is expressed as follows:

$$F_m = \frac{(1 + \beta^2) \cdot Precision \cdot Recall}{\beta^2 \cdot Precision + Recall} \quad (15)$$

where  $\beta^2 = 0.3$  emphasizes the importance of precision, suggested by [46]. The *Precision* is the ratio of the correctly predicted foreground pixels to the totally predicted foreground pixels. The *Recall* is the ratio of the correctly predicted foreground pixels to the ground truth. The mean value of the predicted saliency map is doubled as the threshold to binarize the saliency map, and then F-measure can be computed and marked as  $F_m$ . In addition, we follow [47] to compute the weighted F-measure as another metric marked as  $wF$ . For PR curve, we equally divide the range of saliency score to  $x$  parts as the thresholds to binarize the predicted saliency map and

TABLE I

PERFORMANCE COMPARISON WITH 12 METHODS ON THREE TESTING DATASETS. THE BEST SCORES ARE HIGHLIGHTED IN **RED**, THE SECOND BEST SCORES ARE HIGHLIGHTED IN **GREEN**, AND THE THIRD BEST SCORES ARE HIGHLIGHTED IN **BLUE**.

Methods	VT821					VT1000					VT5000				
	<i>Em</i>	<i>Sm</i>	<i>Fm</i>	<i>MAE</i>	<i>wF</i>	<i>Em</i>	<i>Sm</i>	<i>Fm</i>	<i>MAE</i>	<i>wF</i>	<i>Em</i>	<i>Sm</i>	<i>Fm</i>	<i>MAE</i>	<i>wF</i>
MTMR	0.815	0.725	0.662	0.108	0.462	0.836	0.706	0.715	0.119	0.485	0.795	0.680	0.595	0.114	0.397
M3S-NIR	<b>0.859</b>	0.723	0.734	0.140	0.407	0.827	0.726	0.717	0.145	0.463	0.780	0.652	0.575	0.168	0.327
SGDL	0.847	0.765	0.730	0.085	0.583	0.856	0.787	0.764	0.090	0.652	0.824	0.750	0.672	0.089	0.559
ADF	0.842	0.81	0.716	0.077	0.627	0.921	<b>0.910</b>	0.847	0.034	0.804	<b>0.891</b>	<b>0.864</b>	<b>0.778</b>	<b>0.048</b>	0.722
DMRA	0.691	0.666	0.577	0.216	0.546	0.801	0.784	0.716	0.124	0.699	0.696	0.672	0.562	0.195	0.532
S2MA	0.834	<b>0.829</b>	0.723	0.081	<b>0.702</b>	0.914	<b>0.921</b>	<b>0.852</b>	<b>0.029</b>	<b>0.850</b>	0.869	<b>0.855</b>	0.751	0.055	0.734
PFA	0.756	0.761	0.592	0.096	0.526	0.809	0.813	0.688	0.078	0.635	0.737	0.748	0.563	0.099	0.498
R3Net	0.803	0.782	0.681	0.081	0.656	0.903	0.886	0.835	0.037	0.831	0.856	0.812	0.729	0.059	0.703
BASNet	<b>0.856</b>	0.823	<b>0.735</b>	<b>0.067</b>	<b>0.716</b>	<b>0.923</b>	0.909	0.847	<b>0.030</b>	<b>0.861</b>	0.878	0.839	0.764	0.054	<b>0.742</b>
PoolNet	0.811	0.788	0.652	0.082	0.573	0.852	0.849	0.751	0.063	0.690	0.809	0.788	0.643	0.080	0.570
CPD	0.843	0.818	0.718	0.079	0.686	<b>0.923</b>	0.907	<b>0.863</b>	0.031	0.844	<b>0.894</b>	<b>0.855</b>	<b>0.787</b>	<b>0.046</b>	<b>0.748</b>
EGNet	<b>0.856</b>	<b>0.830</b>	<b>0.726</b>	<b>0.063</b>	0.662	<b>0.922</b>	<b>0.910</b>	0.848	0.033	0.817	0.888	0.853	0.775	0.050	0.712
SiamDecoder	<b>0.895</b>	<b>0.871</b>	<b>0.804</b>	<b>0.045</b>	<b>0.760</b>	<b>0.933</b>	<b>0.915</b>	<b>0.882</b>	<b>0.027</b>	<b>0.856</b>	<b>0.897</b>	<b>0.868</b>	<b>0.801</b>	<b>0.043</b>	<b>0.763</b>

then we calculate corresponding *Precision* and *Recall*. In our evaluation code, we set  $x$  to 20. Thus 20 F-measure values can be calculated and the PR curve can be plotted.

The formula of mean absolute error (*MAE*) is expressed as follows:

$$MAE = \frac{1}{T} \sum_{i=1}^T |S_i - Y_i| \quad (16)$$

where  $S_i$  is a predicted saliency map and  $Y_i$  is the ground truth.  $T$  is the total number of pixels in a map. Thus *MAE* can evaluate the difference between the predicted map and its ground truth. We average all the *MAE* values of test samples as another evaluation metric.

S-measure( $S_m$ ) is used to evaluate the similarity of spatial structure, which combines the region-aware structural similarity  $S_r$  and the object-aware structural similarity  $S_o$ :

$$S_m = \alpha * S_o + (1 - \alpha) * S_r \quad (17)$$

where we set  $\alpha = 0.5$ , more details are introduced in [48].

E-measure( $E_m$ ) is an enhanced alignment measure, proposed recently in [44], which can jointly capture statistic information in image level and matching information in pixel level. By using all above metrics, we can make a comprehensive evaluation of our method.

### C. Comparison with State-of-the-Art Methods

We compare our method with 12 existing methods as follows. Three traditional RGBT SOD methods are SDGL[7], MTMR[5] and M3S-NIR[22]. A deep learning based RGBT SOD method is ADF [8]. Two deep learning based RGBD SOD methods are DMRA [25] and S2MA [49]. And six deep learning based single-modality SOD methods include R3Net [16], PFA [50], CPD [17], EGNet [18], PoolNet [41] and BASNet [51]. To keep the architectures of those single-modality SOD methods well, we apply early fusion strategy

to them for fairness. In addition, it should be mentioned that our method doesn't use any post-processing such as fully connected conditional random fields (CRF) [52] used in R3Net[16].

1) *Quantitative evaluation*: Table I shows the results of our method and other eleven methods on our testing sets. First, it can be seen that our method outperforms well against the existing four RGBT SOD methods with the above metrics. Especially in VT821, our method shows tremendous superiority. The performance of three traditional methods are inferior to the deep learning based methods, which is mainly caused by the weakness of feature representations and the limitation of super-pixel representations.

Second, DMRA [25] is a state-of-the-art RGBD SOD method which has been proven to be effective on RGBD dataset. It uses the middle fusion strategy to fuse two modalities. We train it on VT5000 training set, but it shows the poorer performance on RGBT data. The S2MA [49] is the latest RGBD SOD method. From the Table I, we can find that it can also perform well on RGBT SOD datasets. We have made an analysis that the RGBD SOD task is different from RGBT as the former focuses on modalities complementary and the depth maps are used as auxiliary information, while the later focuses on joint inferring to eliminate the bias between modalities and the thermal maps are with equivalent importance. Therefore RGBD methods can be used on RGBT task, but it is not impeccable. Although DMRA symmetrically fuses features of two modalities, it also adopts a depth-specific module to adjust the features. However, the thermal maps can not be used for that.

Third, we study six single-modality SOD methods, which have the most advanced performance. Because most of visible images have useful information, these methods also work well on simple cases. The early fusion strategy regards two modal-



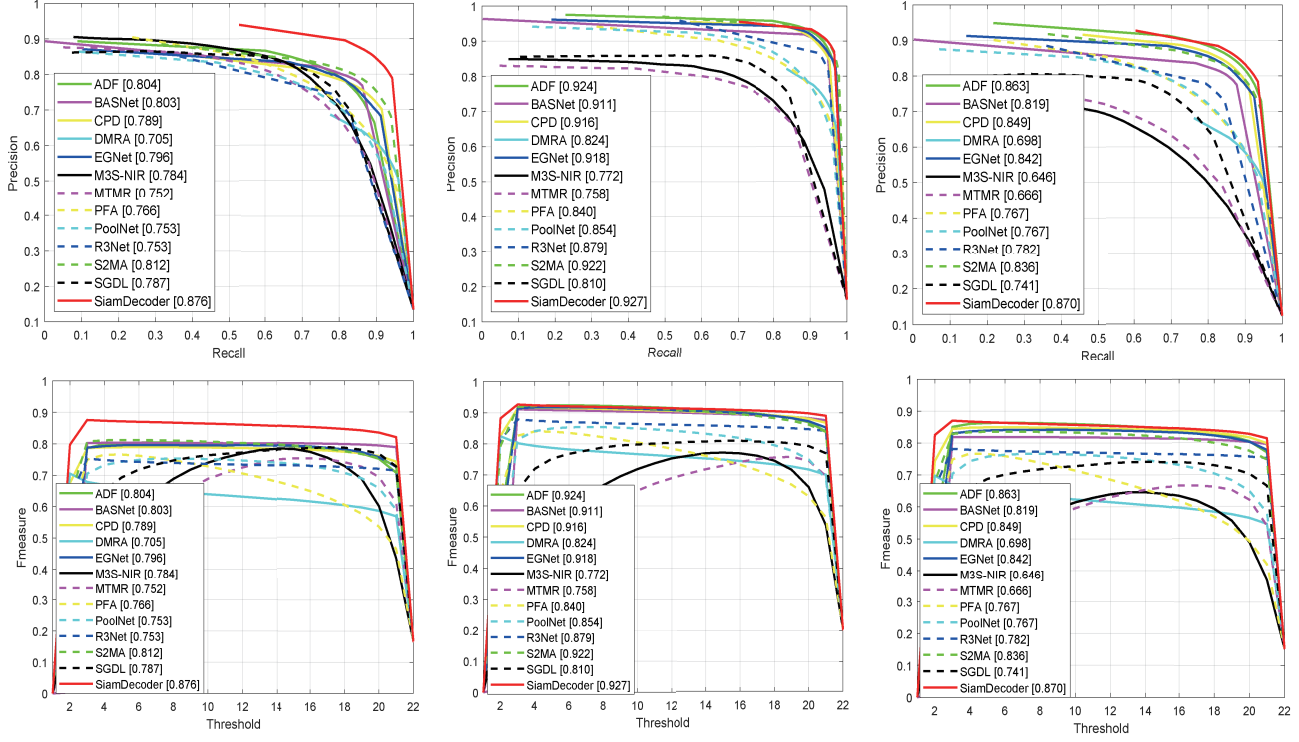


Fig. 4. The first row is PR curve and the second row is F-measure curve. From left to right, the figures are on VT821, VT1000 and VT5000 testing datasets respectively.

ities as a integrated information. The relationship between modalities can be explored in encoding phase, and the modal complementarity can thus also be achieved. Then benefiting from the various advanced segmentation tricks, these methods also work well on RGBT SOD. A further study for the performance of our method will be taken in the ablation experiments.

2) *Qualitative evaluation:* The qualitative comparison can be seen in Fig. 5. We can see our method outperforms all comparison methods in the challenging image pairs. Our network has considered the specialties of two modalities and reasonably integrated features with multi-type cues. Although one of modalities is useless, the other modality is rarely affected by the destructive information. When both of two modalities are informative, our network can take advantage of the complementarity of two modalities to gain more reliable relevance in pixels and make a consistent prediction by suppressing the bias. Even both of modalities are unreliable such as the 8th and 9th columns in Fig. 5, our method can combine the useful information in two modalities to make a better prediction. Those advanced SOD methods work well in informative visible images, but they can't deal with the images with deficiency and semantic ambiguity. As we can see in Fig. 5, single-modality SOD methods with early fusion strategy are impressionable to noise. Therefore they always detect the extra wrong pixels or miss the correct pixels.

The traditional RGBT methods can accurately detect the salient region but they always have lower confidence. The deep learning based RGBT and RGBD methods have better saliency

maps and our method is more robust in challenging cases.

3) *Analysis of PR curves and F-measure curves:* The PR curves and F-measure curves of above-mentioned methods on all testing sets are shown in Fig. 4. We can see that our method always outperforms the comparison methods especially in VT821. We calculate the max F-measure scores and present them in the legends. In PR curves, we can observe that most of methods hold a higher *Precision* while the *Recall* is very low, which means these method can only predict the small parts of the salient regions with a high confidence. Therefore the *Recall* is lower when the threshold is very high. But our method has no such problem, which means our predicted saliency maps always show a consistent confidence in salient regions. In F-measure curves, the horizontal axis represents the threshold indexes as we select 20 thresholds uniformly-spaced in the range of scores. We can observe that our method shows the stable F-measure scores as the threshold changes, which implies our saliency maps has a large range between the mean value of foreground scores and background scores. In summary, our network can make a more decisive inference than comparison methods.

4) *Challenge-based quantitative evaluation:* We further make a study on all challenges labeled by VT5000. The quantitative comparisons are presented in Table II. The first eleven columns are the challenge attributes and the last two columns are quality attributes which present the deficient modalities. As we can see in Table II, our method has the best performance on all challenges. We compute the mean F-measure scores of all methods on thirteen challenges and use



TABLE II  
PERFORMANCE COMPARISON WITH 12 METHODS ON 11 CHALLENGES AND 2 QUALITY ATTRIBUTIONS. THE BEST SCORES ARE HIGHLIGHTED IN **RED**, THE SECOND BEST SCORES ARE HIGHLIGHTED IN **GREEN**, AND THE THIRD BEST SCORES ARE HIGHLIGHTED IN **BLUE**.

	BSO	CB	CIB	IC	LI	MSO	OF	SSO	SA	TC	BW	Bad RGB	Bad T
DMRA	0.795	0.675	0.736	0.662	0.716	0.663	0.690	0.355	0.675	0.652	0.648	0.687	0.640
S2MA	<b>0.873</b>	0.817	0.860	0.794	<b>0.859</b>	0.805	<b>0.844</b>	0.735	0.811	0.810	0.773	<b>0.825</b>	<b>0.810</b>
PFA	0.803	0.746	0.743	0.735	0.747	0.73	0.754	0.689	0.725	0.763	0.666	0.730	0.755
R3Net	0.829	0.790	0.821	0.74	0.787	0.775	0.757	0.657	0.727	0.725	0.747	0.735	0.715
BASNet	0.859	0.808	0.824	0.774	0.832	0.799	0.816	0.716	0.763	0.792	0.768	0.787	0.787
PoolNet	0.801	0.725	0.741	0.720	0.753	0.708	0.761	0.658	0.728	0.718	0.749	0.732	0.716
CPD	<b>0.873</b>	<b>0.845</b>	<b>0.863</b>	0.811	0.840	0.829	0.823	<b>0.766</b>	<b>0.828</b>	<b>0.811</b>	<b>0.793</b>	0.809	0.801
EGNet	0.874	0.838	0.856	<b>0.817</b>	0.848	<b>0.818</b>	0.819	0.700	0.794	0.790	0.772	0.792	0.775
MTMR	0.666	0.574	0.579	0.562	0.688	0.621	0.707	0.697	0.652	0.567	0.605	0.668	0.562
M3S-NIR	0.645	0.563	0.571	0.554	0.700	0.597	0.709	0.600	0.609	0.560	0.636	0.557	0.640
SGDL	0.755	0.703	0.693	0.680	0.740	0.709	0.74	0.755	0.656	0.674	0.641	0.672	0.662
ADF	<b>0.881</b>	<b>0.853</b>	<b>0.862</b>	<b>0.834</b>	<b>0.868</b>	<b>0.839</b>	<b>0.839</b>	<b>0.805</b>	<b>0.837</b>	<b>0.841</b>	<b>0.804</b>	<b>0.820</b>	<b>0.832</b>
SiamDecoder	<b>0.891</b>	<b>0.869</b>	<b>0.869</b>	<b>0.840</b>	<b>0.878</b>	<b>0.843</b>	<b>0.861</b>	<b>0.813</b>	<b>0.855</b>	<b>0.850</b>	<b>0.812</b>	<b>0.844</b>	<b>0.838</b>

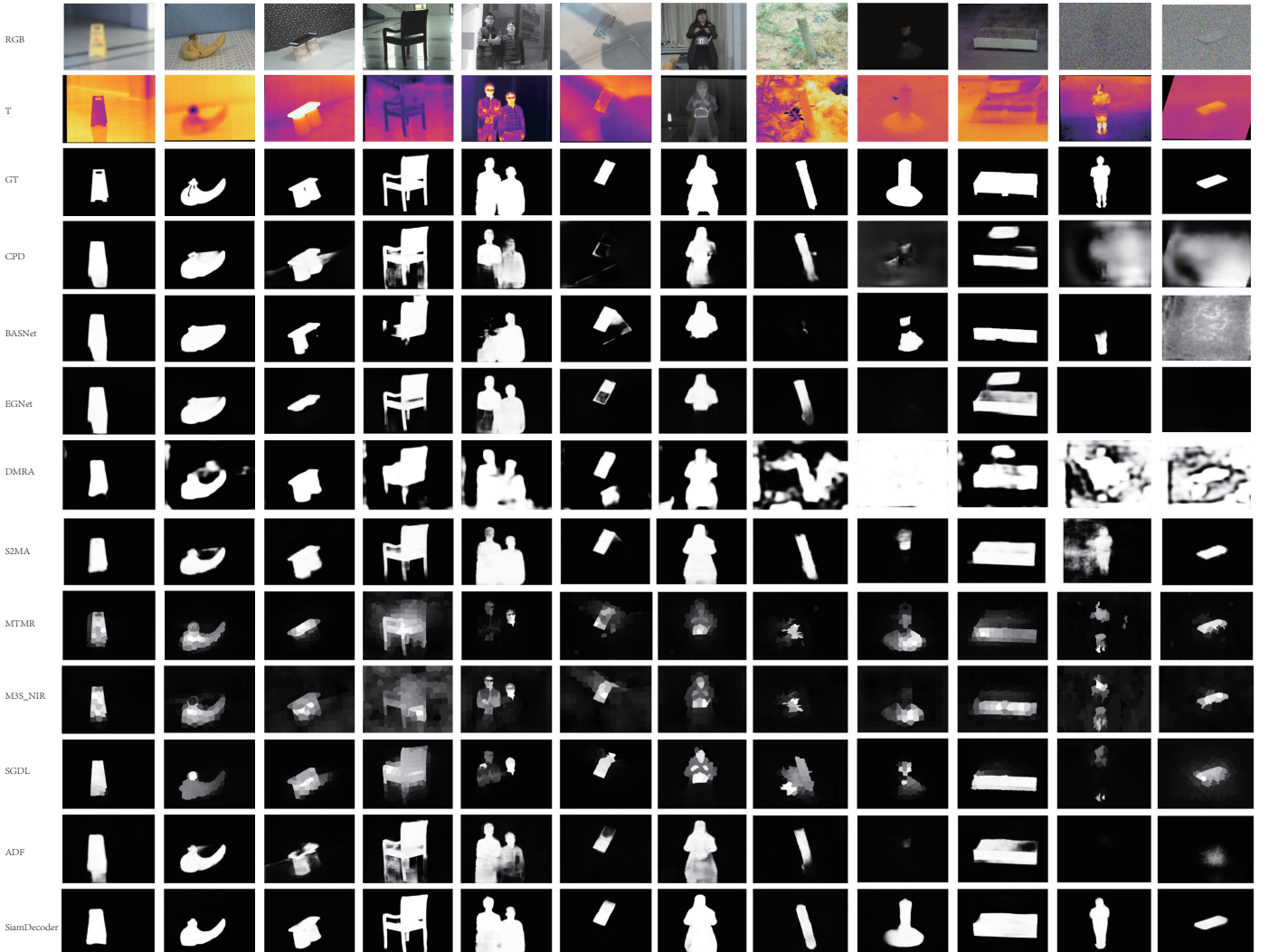


Fig. 5. Qualitative comparison of the proposed method with other methods. We select 12 RGBT image pairs with diverse challenges to compare the quality of the predicted maps.

TABLE III  
ABLATION STUDIES WITH DIFFERENT SETUPS. *w/o* MEANS DISABLING THE CORRESPONDING COMPONENT.

	VT821				VT1000				VT5000			
	<i>Sm</i>	<i>Em</i>	<i>Fm</i>	<i>MAE</i>	<i>Sm</i>	<i>Em</i>	<i>Fm</i>	<i>MAE</i>	<i>Sm</i>	<i>Em</i>	<i>Fm</i>	<i>MAE</i>
<i>w/o</i> $\mathcal{L}_d$	0.863	0.881	0.790	0.048	0.901	0.912	0.868	0.030	0.860	0.883	0.783	0.047
<i>w/o</i> Noise Data	0.852	0.878	0.776	0.052	0.907	0.928	0.871	0.029	0.856	0.891	0.789	0.046
<i>w/o</i> Global Interaction	0.857	0.873	0.771	0.057	0.892	0.906	0.843	0.036	0.852	0.874	0.764	0.051
<i>w/o</i> Modality Interaction	0.864	0.882	0.781	0.050	0.898	0.911	0.846	0.031	0.861	0.890	0.792	0.045
Single Decoder	0.862	0.884	0.779	0.051	0.907	0.921	0.868	0.031	0.852	0.875	0.774	0.049
SiamDecoder_VGG16	<b>0.871</b>	<b>0.895</b>	<b>0.804</b>	<b>0.045</b>	0.915	<b>0.933</b>	<b>0.882</b>	0.027	0.868	0.897	0.801	<b>0.043</b>
SiamDecoder_ResNet50	<b>0.871</b>	0.882	0.790	0.047	<b>0.921</b>	0.927	0.875	<b>0.025</b>	<b>0.874</b>	0.896	0.800	0.044
SiamDecoder_ResNet50+	0.870	0.882	0.796	0.049	<b>0.921</b>	0.929	0.881	0.027	<b>0.874</b>	<b>0.900</b>	<b>0.810</b>	0.044

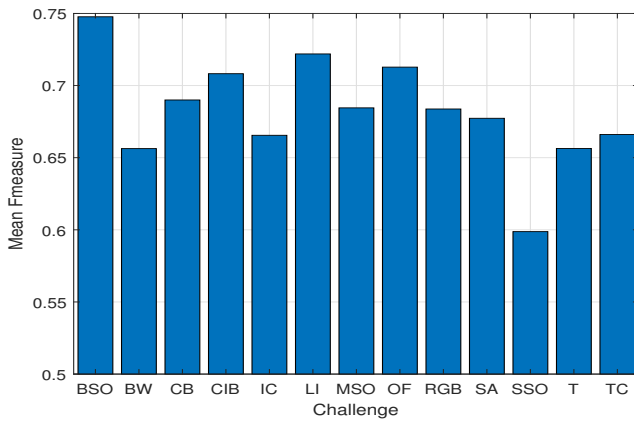


Fig. 6. The statistics of mean F-measure score of all the methods on 13 challenges.

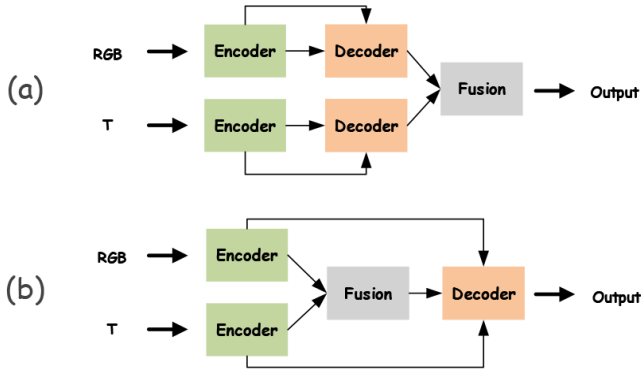


Fig. 7. (a) Framework of 'w/o Modality Interaction'. (b) Framework of 'Single Decoder'.

a histogram to present them in Fig. 6. The low illumination (LI), small salient object (SSO) and bad weather (BW) seem to be the most three difficult challenges. Because these cases are more likely to lead a deficient modality or ambiguous context. Once the discrepancy between modalities, the joint inference becomes difficult.

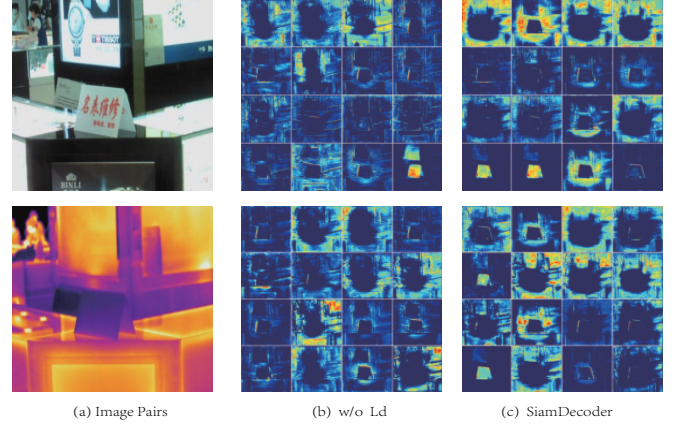


Fig. 8. Without the supervision on two branches of Siamese decoder. The feature maps of two decoder streams are less likely to be consistent.

#### D. Ablation Study

In this section, we mainly study the effects of different configurations on network performance, as shown in Table III. We first explore the supervisions on the two branches of Siamese decoder, which is used for guiding the modal complementarity and eliminating the modality bias. Then we study the modality interaction and global context interaction of our network. Since the hierarchical features interaction is necessary for decoder, we do not study for it. Without the modality interaction, our network is degenerated into an original late fusion based framework as shown in the (a) of Fig. 7. Furthermore, we study the single decoder stream with the middle fusion strategy on our network as shown in the (b) of Fig. 7. Then we disable the used data augmentation strategy and verify the effectiveness of it. Finally, we replace VGG16 by ResNet50 [53] as the encoder block of our network. Since the features extracted by ResNet50 have lower resolutions, we further add a MIB block to fusion the bottom encoded features. We will make detailed analysis of these factors in following parts.

1) *Supervision effect in Siamese decoder:* In Tabel III, '*w/o*  $\mathcal{L}_d$ ' represents that we don't use the output features of the two decoder branches to predict the saliency maps, and the supervision only exists in the final predicted saliency map. As

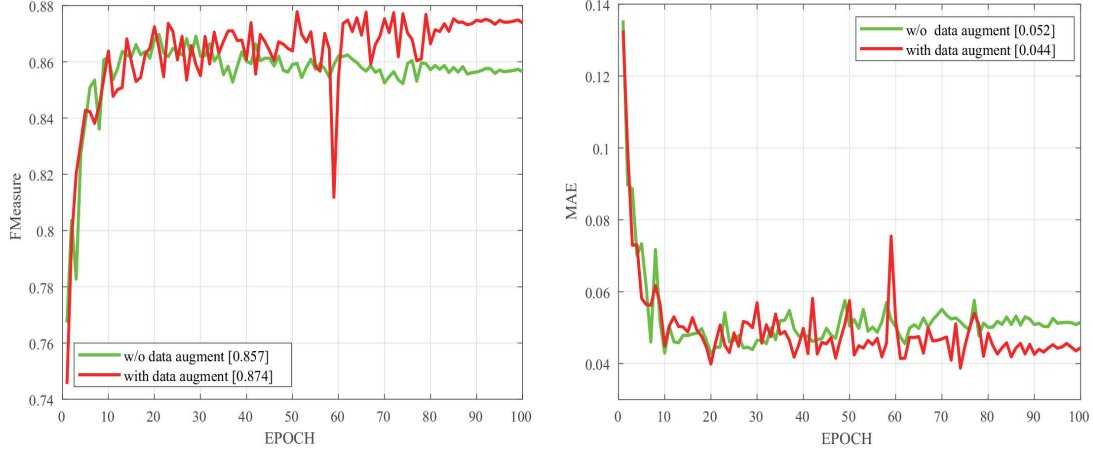


Fig. 9. Max F-measure scores and  $MAE$  on VT821 in the whole training procedure to verify the effectiveness of the used data augmentation strategy.

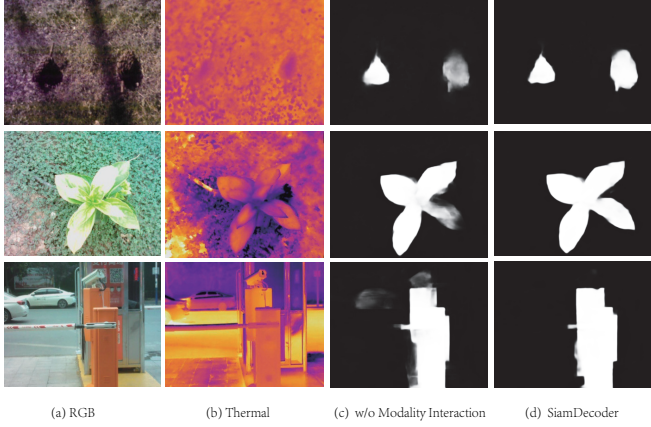


Fig. 10. Comparison on saliency maps of our network with/without the modality interaction.

we can see in Tabel III, the performance in four metrics have declined without  $\mathcal{L}_d$ . We visualize the feature maps of final decoder step in Figure 8. When the supervisions are absent, the ability of modality complementarity is weakened. Therefore Siamese decoder can not cooperate well though the multiple interactions exist.

2) *Effect of MIB*: In our network, the two decoder streams consist of three MIBs. Each MIB performs the interactions and fusions of multi-type cues. Therefore, to evaluate the ability of MIB, we should explore the usefulness of global information interaction and modality interaction. The global contexts play a vital role in our network because we rely on it to suppress the long range background noises and highlight foreground regions. In addition, it also provide a coarse modality relevance, which is helpful for seeking common salient regions. Without the global context interaction, the scores in all the metrics decline more than 1.5%.

The modality interaction are conducted in all the decoder steps. Without these interactions, the framework is degraded into a common late fusion based methods shown in Figure 7. We compare the saliency maps of our network with and without this interaction in Figure 10. As we can see, the saliency

maps have larger confidence both in foreground regions and background regions when the modality interaction exists. If we disable modality interaction in Siamese decoder and only fusion the output features of Siamese decoder to predict the saliency map, the network can not withstand the noise coming from one deficient modality and has limited ability to eliminate the modality bias, thus leading the uncertain results.

3) *Effect of Siamese decoder network*: We further achieve a single decoder based version of our network shown in (b) of Figure 7. This framework maintains the global context interaction and then directly concatenate the hierarchical encoded features of two modalities to interact in a single decoder stream. From the comparisons on different metrics, we can find the performance of this method is obviously inferior to our baseline, which verifies the effectiveness of our Siamese decoder network.

4) *Effect of noisy data augmentation*: Finally, we compare the performance of our network trained with or without noisy data augmentation. As we can see in Table III, training with noisy data can improve the performance more than 2%. We present the results of max F-measure and  $MAE$  in the whole training procedure in Figure 9. The network converges after 90 epochs, and we can find the stable gains when our network trained with noisy data augmentation.

5) *Effect of different backbones*: We replace VGG16 by ResNet50 as the backbone of our network. This setup is marked as "SiamDecoder\_ResNet50" in Table III. We all know that ResNet50 has stronger ability in feature representation than VGG16, but the performance of two backbones have little difference as we can find in Table III. This is mainly caused by the lower resolution of features extracted by ResNet50. The resolution of the output is half of VGG16, which has less spatial details and coarser structure. Since the features extracted by ResNet50 have lower resolutions, we further add a MIB block to fusion the bottom encoded features, which is marked as "SiamDecoder\_ResNet50+". The output has higher resolution and more details through the extra MIB, but more background details are also integrated into it. Thus, the "SiamDecoder\_ResNet50+" can improve the performance

TABLE IV

PERFORMANCE COMPARISON WITH TEN METHODS ON 5 RGBD SOD DATASETS. THE BEST SCORES ARE HIGHLIGHTED IN **RED**, THE SECOND BEST SCORES ARE HIGHLIGHTED IN **GREEN**, AND THE THIRD BEST SCORES ARE HIGHLIGHTED IN **BLUE**.

	DES				LFSD				SIP				SSD				STERE			
	<i>Sm</i>	<i>Em</i>	<i>Fm</i>	<i>MAE</i>	<i>Sm</i>	<i>Em</i>	<i>Fm</i>	<i>MAE</i>	<i>Sm</i>	<i>Em</i>	<i>Fm</i>	<i>MAE</i>	<i>Sm</i>	<i>Em</i>	<i>Fm</i>	<i>MAE</i>	<i>Sm</i>	<i>Em</i>	<i>Fm</i>	<i>MAE</i>
DF2017	0.752	0.877	0.753	0.093	0.791	0.844	0.806	0.138	0.653	0.794	0.673	0.185	0.747	0.812	0.724	0.142	0.757	0.838	0.742	0.141
PCF2018	0.842	0.912	0.782	0.049	0.794	0.842	0.792	0.112	0.842	0.899	0.825	0.071	0.841	0.886	0.791	0.062	0.875	0.897	0.826	0.064
CTMF2018	0.863	0.911	0.778	0.055	0.796	0.851	0.782	0.119	0.716	0.824	0.684	0.139	0.776	0.838	0.710	0.099	0.848	0.864	0.771	0.086
MMCI2019	0.848	0.904	0.762	0.065	0.787	0.840	0.779	0.132	0.833	0.886	0.795	0.086	0.813	0.860	0.748	0.082	0.873	0.901	0.829	0.068
AFNet2019	0.770	0.874	0.730	0.068	0.738	0.810	0.742	0.133	0.720	0.815	0.705	0.118	0.714	0.803	0.694	0.118	0.825	0.886	0.807	0.075
TANet2019	0.858	0.919	0.795	0.046	0.801	0.845	0.794	0.111	0.835	0.893	0.809	0.075	0.839	0.879	0.767	0.063	0.871	0.906	0.835	0.060
DMRA2019	0.867	0.920	0.806	0.033	0.767	0.824	0.792	0.111	0.800	0.858	0.815	0.088	0.857	0.892	0.821	0.058	0.834	0.899	0.844	0.066
D3Net2020	0.898	0.951	0.870	0.031	0.832	0.833	0.801	0.099	0.86	0.902	0.835	0.063	0.857	0.897	0.814	0.058	0.899	0.920	0.859	0.046
S2MA2020	0.910	0.888	0.776	0.033	0.837	0.863	0.820	0.094	0.872	0.911	0.854	0.057	0.708	0.781	0.633	0.138	0.890	0.907	0.855	0.051
cmSalGAN2020	0.913	0.948	0.869	0.028	0.830	0.870	0.831	0.097	0.865	0.902	0.849	0.064	0.791	0.851	0.717	0.086	0.896	0.914	0.863	0.050
SiamDecoder_VGG16	0.916	0.972	0.913	0.022	0.846	0.875	0.839	0.080	0.862	0.908	0.856	0.057	0.814	0.890	0.785	0.066	0.894	0.922	0.870	0.041
SiamDecoder_ResNet50	0.903	0.962	0.906	0.025	0.858	0.884	0.852	0.074	0.869	0.913	0.866	0.054	0.817	0.904	0.802	0.062	0.895	0.921	0.872	0.043
SiamDecoder_ResNet50+	0.915	0.971	0.917	0.022	0.85	0.882	0.844	0.080	0.883	0.926	0.879	0.047	0.837	0.901	0.805	0.056	0.901	0.927	0.881	0.040

in some aspects but it is not optimal setup. These three setups of our network can show their superiority in different scenes and all of them outperform the state-of-the-art methods.

### E. Comparison with RGBD SOD Methods

We observe that some RGBD SOD methods also take similar manners to manage the RGB and depth data rather than only regarding the depth as auxiliary information. Therefore, to verify the generalization ability of our model, we can also perform it on RGBD SOD task and compare with these RGBD SOD methods.

1) *Dataset*: To fully verify the effectiveness of the our method on RGBD SOD, we perform the experiments on seven RGBD SOD benchmark datasets. The NJU2K [54] contains 1,985 RGBD image pairs with labeled saliency maps, which are collected from the Internet and 3D movies or taken by a Fuji W3 stereo camera. NLPR [55] collects 1,000 RGBD image pairs captured by Microsoft Kinect. DES [56] is also named RGBD135 since it contains 135 RGBD image pairs about indoor scenes collected by Microsoft Kinect. LFSD [57] has 100 image pairs with depth information and labelled ground truths. SSD [58] is also a small dataset that contains 80 image pairs picked up from three stereo movies. SIP [59] collect 1,000 image pairs in outdoor scenarios and it has many challenging situations. STERE [60] also contains 1000 various image pairs which include real-world scenes and virtual scenes.

2) *Experiment setup*: We randomly sample 1485 image pairs and 700 image pairs from the NJU2K [54] and NLPR [55] datasets as the training set, which is common used in RGBD SOD methods. For fairness, we test on DES, LFSD, SIP, SSD and STERE.

We compare 10 applicable RGBD SOD methods which include DF [33], PCF [31], CTMF [61], MMCI [62], AFNet [28], TANet [30], DMRA [25], D3Net [59], S2MA [49] and cmSalGAN [63]. These methods relatively equally deal with RGB and depth, and thus it is fair to compare with our methods. We use the available codes with provided models to predict saliency maps or directly use the provided saliency maps to make evaluations on S-measure(*Sm*), E-measure(*Em*), F-measure(*Fm*) and *MAE*. For our method, we follow the experimental setup of RGBT SOD except that the input size is adjust to 256 and the noisy data augmentation strategy is unused since the RGBD image pairs have less possibility of catching invalid informations.

3) *Quantitative evaluation*: As we can see in Table IV, our method also performs well on RGBD datasets. Compared with ten RGBD SOD methods, our method can even surpass the most of them. On SSD, the performance doesn't follow the law of other datasets, which is mainly caused by the less samples and lower otherness in samples of SSD. Thus the performance shows lower stability. On the other datasets, our method can basically outperform other compared methods. And our method based on ResNet50 [53] with four MIBs can further improve the performance on larger datasets or higher resolution samples like SIP and STERE.

## V. CONCLUSION

In this paper, we propose a multi-interactive Siamese decoder network for RGBT SOD. Considering the different relevance among the dual modalities, the encoded hierarchical features and the global contexts, we design a Siamese decoder network with cascaded multi-interactive modules to achieve sufficient fusion of different source data. The proposed network can prevent information of two modalities from excessive



influence by each other during the interactions. And with the same supervision, two decoder branches trend to be consistent, and the balanced computation of dual modalities is thus achieved implicitly. Experimental results show the superiority of our method for RGBT SOD. From the challenge-based experiments we can observe some difficulties of RGBT SOD task, such as small objects. We will explore new models in our framework to address these difficulties in the future.

## REFERENCES

- [1] C. Li, H. Cheng, S. Hu, X. Liu, J. Tang, and L. Lin, "Learning collaborative sparse representation for grayscale-thermal tracking," *IEEE Transactions on Image Processing*, vol. 25, no. 12, pp. 5743–5756, 2016.
- [2] C. Li, X. Liang, Y. Lu, N. Zhao, and J. Tang, "Rgb-t object tracking: benchmark and baseline," *Pattern Recognition*, 2019.
- [3] M. Ye, Z. Wang, X. Lan, and P. C. Yuen, "Visible thermal person re-identification via dual-constrained top-ranking," in *Proceedings of the International Joint Conference on Artificial Intelligence*, 2018.
- [4] Y. Hao, N. Wang, J. Li, and X. Gao, "Hsme: Hypersphere manifold embedding for visible thermal person re-identification," in *Proceedings of the AAAI Conference on Artificial Intelligence*, 2019.
- [5] G. Wang, C. Li, Y. Ma, A. Zheng, J. Tang, and B. Luo, "Rgb-t saliency detection benchmark: Dataset, baselines, analysis and a novel approach," in *Chinese Conference on Image and Graphics Technologies*, 2018.
- [6] J. Tang, D. Fan, X. Wang, Z. Tu, and C. Li, "Rgbt salient object detection: Benchmark and a novel cooperative ranking approach," *IEEE Transactions on Circuits and Systems for Video Technology*, vol. PP, no. 99, pp. 1–1, 2019.
- [7] Z. Tu, T. Xia, C. Li, X. Wang, Y. Ma, and J. Tang, "Rgb-t image saliency detection via collaborative graph learning," *IEEE Transactions on Multimedia*, vol. 22, no. 1, pp. 160–173, 2019.
- [8] Z. Tu, Y. Ma, Z. Li, C. Li, J. Xu, and Y. Liu, "Rgbt salient object detection: A large-scale dataset and benchmark," *arXiv preprint arXiv:2007.03262*, 2020.
- [9] Q. Zhang, N. Huang, L. Yao, D. Zhang, C. Shan, and J. Han, "Rgb-t salient object detection via fusing multi-level cnn features," *IEEE Transactions on Image Processing*, vol. 29, pp. 3321–3335, 2020.
- [10] L. Wang, H. Lu, X. Ruan, and M.-H. Yang, "Deep networks for saliency detection via local estimation and global search," in *Proceedings of the IEEE Conference on Computer Vision and Pattern Recognition*, 2015.
- [11] N. Liu and J. Han, "Dhsnet: Deep hierarchical saliency network for salient object detection," in *Proceedings of the IEEE Conference on Computer Vision and Pattern Recognition*, 2016.
- [12] L. Wang, L. Wang, H. Lu, P. Zhang, and X. Ruan, "Saliency detection with recurrent fully convolutional networks," in *Proceedings of the European Conference on Computer Vision*, 2016.
- [13] Q. Hou, M. Cheng, X. Hu, A. Borji, Z. Tu, and P. H. Torr, "Deeply supervised salient object detection with short connections," in *Proceedings of the IEEE Conference on Computer Vision and Pattern Recognition*, 2017.
- [14] Z. Luo, A. Mishra, A. Achkar, J. Eichel, S. Li, and P.-M. Jodoin, "Non-local deep features for salient object detection," in *Proceedings of the IEEE Conference on Computer Vision and Pattern Recognition*, 2017.
- [15] N. Liu, J. Han, and M.-H. Yang, "Picanet: Learning pixel-wise contextual attention for saliency detection," in *Proceedings of the IEEE Conference on Computer Vision and Pattern Recognition*, 2018.
- [16] Z. Deng, X. Hu, L. Zhu, X. Xu, J. Qin, G. Han, and P.-A. Heng, "R3net: Recurrent residual refinement network for saliency detection," in *Proceedings of the 27th International Joint Conference on Artificial Intelligence*, 2018.
- [17] Z. Wu, L. Su, and Q. Huang, "Cascaded partial decoder for fast and accurate salient object detection," in *Proceedings of the IEEE Conference on Computer Vision and Pattern Recognition*, 2019.
- [18] J. Zhao, J. Liu, D. Fan, Y. Cao, J. Yang, and M. Cheng, "Egnet: Edge guidance network for salient object detection," in *Proceedings of the IEEE International Conference on Computer Vision*, 2019.
- [19] J. Wei, S. Wang, and Q. Huang, "F3net: Fusion, feedback and focus for salient object detection," 2020.
- [20] C. Li, C. Zhu, Y. Huang, J. Tang, and L. Wang, "Cross-modal ranking with soft consistency and noisy labels for robust rgb-t tracking," in *Proceedings of the European Conference on Computer Vision*, 2018.
- [21] C. Li, A. Lu, A. Zheng, Z. Tu, and J. Tang, "Multi-adaptor rgbt tracking," in *Proceedings of the IEEE International Conference on Computer Vision Workshops*, 2019.
- [22] Z. Tu, T. Xia, C. Li, Y. Lu, and J. Tang, "M3s-nir: Multi-modal multi-scale noise-insensitive ranking for rgb-t saliency detection," in *IEEE Conference on Multimedia Information Processing and Retrieval*, 2019.
- [23] Y. Ding, Z. Liu, M. Huang, R. Shi, and X. Wang, "Depth-aware saliency detection using convolutional neural networks," *Journal of Visual Communication and Image Representation*, vol. 61, pp. 1–9, 2019.
- [24] Y. Piao, Z. Rong, M. Zhang, W. Ren, and H. Lu, "A2dele: Adaptive and attentive depth distiller for efficient rgb-d salient object detection," in *Proceedings of the IEEE Conference on Computer Vision and Pattern Recognition*, 2020.
- [25] Y. Piao, W. Ji, J. Li, M. Zhang, and H. Lu, "Depth-induced multi-scale recurrent attention network for saliency detection," in *Proceedings of the IEEE International Conference on Computer Vision*, 2019.
- [26] M. Zhang, W. Ren, Y. Piao, Z. Rong, and H. Lu, "Select, supplement and focus for rgb-d saliency detection," in *Proceedings of the IEEE Conference on Computer Vision and Pattern Recognition*, 2020.
- [27] Y. Pang, L. Zhang, X. Zhao, and H. Lu, "Hierarchical dynamic filtering network for rgb-d salient object detection," *Proceedings of the European Conference on Computer Vision*, 2020.
- [28] N. Wang and X. Gong, "Adaptive fusion for rgb-d salient object detection," *IEEE Access*, vol. 7, pp. 55 277–55 284, 2019.
- [29] D. Liu, Y. Hu, K. Zhang, and Z. Chen, "Two-stream refinement network for rgb-d saliency detection," in *Proceedings of the IEEE International Conference on Image Processing*, 2019.
- [30] H. Chen and Y. Li, "Three-stream attention-aware network for rgb-d salient object detection," *IEEE Transactions on Image Processing*, vol. 28, no. 6, pp. 2825–2835, 2019.
- [31] H. Chen and Y. Li, "Progressively complementarity-aware fusion network for rgb-d salient object detection," in *Proceedings of the IEEE Conference on Computer Vision and Pattern Recognition*, 2018.
- [32] K. Fu, D. Fan, G. Ji, and Q. Zhao, "Jl-dcf: Joint learning and densely-cooperative fusion framework for rgb-d salient object detection," in *Proceedings of the IEEE Conference on Computer Vision and Pattern Recognition*, 2020.
- [33] L. Qu, S. He, J. Zhang, J. Tian, Y. Tang, and Q. Yang, "Rgb-d salient object detection via deep fusion," *IEEE Transactions on Image Processing*, vol. 26, no. 5, pp. 2274–2285, 2017.
- [34] H. Song, Z. Liu, H. Du, G. Sun, O. Le Meur, and T. Ren, "Depth-aware salient object detection and segmentation via multiscale discriminative saliency fusion and bootstrap learning," *IEEE Transactions on Image Processing*, vol. 26, no. 9, pp. 4204–4216, 2017.
- [35] Z. Liu, S. Shi, Q. Duan, W. Zhang, and P. Zhao, "Salient object detection for rgb-d image by single stream recurrent convolution neural network," *Neurocomputing*, vol. 363, pp. 46–57, 2019.
- [36] K. Simonyan and A. Zisserman, "Very deep convolutional networks for large-scale image recognition," *arXiv preprint arXiv:1409.1556*, 2014.
- [37] H. Zhao, J. Shi, X. Qi, X. Wang, and J. Jia, "Pyramid scene parsing network," in *Proceedings of the IEEE Conference on Computer Vision and Pattern Recognition*, 2017.
- [38] S. Woo, J. Park, J.-Y. Lee, and I. So Kweon, "Cbam: Convolutional block attention module," in *Proceedings of the European Conference on Computer Vision*, 2018.
- [39] S. Ioffe and C. Szegedy, "Batch normalization: Accelerating deep network training by reducing internal covariate shift," *arXiv preprint arXiv:1502.03167*, 2015.
- [40] V. Nair and G. E. Hinton, "Rectified linear units improve restricted boltzmann machines," in *Proceedings of the International Conference on Machine Learning*, 2010.
- [41] J. Liu, Q. Hou, M. Cheng, J. Feng, and J. Jiang, "A simple pooling-based design for real-time salient object detection," in *Proceedings of the IEEE Conference on Computer Vision and Pattern Recognition*, 2019.
- [42] C. Godard, O. Mac Aodha, and G. J. Brostow, "Unsupervised monocular depth estimation with left-right consistency," in *Proceedings of the IEEE Conference on Computer Vision and Pattern Recognition*, 2017.
- [43] Y. Wang, Y. Yang, Z. Yang, L. Zhao, P. Wang, and W. Xu, "Occlusion aware unsupervised learning of optical flow," in *Proceedings of the IEEE Conference on Computer Vision and Pattern Recognition*, 2018.
- [44] D. P. Fan, C. Gong, Y. Cao, B. Ren, M. M. Cheng, and A. Borji, "Enhanced-alignment measure for binary foreground map evaluation," in *Proceedings of the International Joint Conference on Artificial Intelligence*, 2018.
- [45] F. Perazzi, P. Krähenbühl, Y. Pritch, and A. Hornung, "Saliency filters: Contrast based filtering for salient region detection," in *Proceedings*

- of the *IEEE Conference on Computer Vision and Pattern Recognition*, 2012.
- [46] R. Achanta, S. Hemami, F. Estrada, and S. Susstrunk, “Frequency-tuned salient region detection,” in *Proceedings of the IEEE Conference on Computer Vision and Pattern Recognition*, 2009.
  - [47] R. Margolin, L. Zelnik-Manor, and A. Tal, “How to evaluate foreground maps?” in *Proceedings of the IEEE Conference on Computer Vision and Pattern Recognition*, 2014.
  - [48] D. P. Fan, M. Cheng, Y. Liu, T. Li, and A. Borji, “Structure-measure: A new way to evaluate foreground maps,” in *Proceedings of the IEEE International Conference on Computer Vision*, 2017.
  - [49] N. Liu, N. Zhang, and J. Han, “Learning selective self-mutual attention for rgb-d saliency detection,” in *Proceedings of the IEEE Conference on Computer Vision and Pattern Recognition*, 2020.
  - [50] T. Zhao and X. Wu, “Pyramid feature attention network for saliency detection,” in *Proceedings of the IEEE Conference on Computer Vision and Pattern Recognition*, 2019.
  - [51] X. Qin, Z. Zhang, C. Huang, C. Gao, M. Dehghan, and M. Jagersand, “Basnet: Boundary-aware salient object detection,” in *Proceedings of the IEEE Conference on Computer Vision and Pattern Recognition*, 2019.
  - [52] P. Krähenbühl and V. Koltun, “Efficient inference in fully connected crfs with gaussian edge potentials,” in *Advances in Neural Information Processing Systems*, 2011.
  - [53] K. He, X. Zhang, S. Ren, and J. Sun, “Deep residual learning for image recognition,” in *Proceedings of the IEEE Conference on Computer Vision and Pattern Recognition*, 2016.
  - [54] R. Ju, L. Ge, W. Geng, T. Ren, and G. Wu, “Depth saliency based on anisotropic center-surround difference,” in *Proceedings of the IEEE International Conference on Image Processing*, 2014.
  - [55] H. Peng, B. Li, W. Xiong, W. Hu, and R. Ji, “Rgb-d salient object detection: A benchmark and algorithms,” in *Proceedings of the European Conference on Computer Vision*, 2014.
  - [56] Y. Cheng, H. Fu, X. Wei, J. Xiao, and X. Cao, “Depth enhanced saliency detection method,” in *Proceedings of International Conference on Internet Multimedia Computing and Service*, 2014.
  - [57] N. Li, J. Ye, Y. Ji, H. Ling, and J. Yu, “Saliency detection on light field,” in *Proceedings of the IEEE Conference on Computer Vision and Pattern Recognition*, 2014.
  - [58] C. Zhu and G. Li, “A three-pathway psychobiological framework of salient object detection using stereoscopic technology,” in *Proceedings of the IEEE International Conference on Computer Vision Workshops*, 2017.
  - [59] D. Fan, Z. Lin, Z. Zhang, M. Zhu, and M. Cheng, “Rethinking rgb-d salient object detection: Models, data sets, and large-scale benchmarks,” *IEEE Transactions on Neural Networks and Learning Systems*, 2020.
  - [60] Y. Niu, Y. Geng, X. Li, and F. Liu, “Leveraging stereopsis for saliency analysis,” in *Proceedings of the IEEE Conference on Computer Vision and Pattern Recognition*, 2012.
  - [61] J. Han, H. Chen, N. Liu, C. Yan, and X. Li, “Cnns-based rgb-d saliency detection via cross-view transfer and multiview fusion,” *IEEE transactions on cybernetics*, vol. 48, no. 11, pp. 3171–3183, 2018.
  - [62] H. Chen, Y. Li, and D. Su, “Multi-modal fusion network with multi-scale multi-path and cross-modal interactions for rgb-d salient object detection,” *Pattern Recognition*, vol. 86, pp. 376–385, 2019.
  - [63] B. Jiang, Z. Zhou, X. Wang, J. Tang, and B. Luo, “cmsalgan: Rgb-d salient object detection with cross-view generative adversarial networks,” *IEEE Transactions on Multimedia*, vol. PP, no. 99, pp. 1–1, 2020.